Transport through a network of two-dimensional NbC superconducting crystals connected via weak links

Meng Hao,[1] Chuan Xu,[2] Zhen Liu,[1] Cheng Wang,[1] Zhibo Liu,[2] Su Sun,[2] Hui-Ming Cheng,[2] Wencai Ren,[2,*] and Ning Kang[1,†]

[1]*Key Laboratory for the Physics and Chemistry of Nanodevices and Department of Electronics, Peking University, Beijing 100871, China*
[2]*Shenyang National Laboratory for Materials Science, Institute of Metal Research, Chinese Academy of Sciences, Shenyang 110016, China*

(Received 22 September 2019; revised manuscript received 18 January 2020; accepted 2 March 2020; published 23 March 2020)

Recent progresses in the growth and fabrication techniques for preparing crystalline two-dimensional (2D) superconductors have stimulated intense interest in the studies of the electronic properties of these systems. Here we investigate the superconducting transport properties based on chemical vapor deposition-grown thin NbC crystals consisting of network structures. The 2D character of the superconductivity in individual NbC crystals is revealed by examining the angular dependence of magnetotransport measurements. At low temperatures, the samples show nonmonotonic double-step superconducting transitions as a function of temperature and magnetic field. We demonstrate that the observed transport characteristics can be understood in terms of coupled Josephson junctions forming between isolated NbC crystals, including the effects of Josephson and quasiparticle tunneling. In particular, detailed analysis of the magnetic field-driven transition suggests the existence of quantum flux-creep regime at low temperatures and small magnetic fields in such thin NbC superconducting crystals. Our work underlines the importance of the morphology on the transport properties of 2D superconducting crystals, providing a comprehensive understanding of crystalline 2D superconductors.

DOI: 10.1103/PhysRevB.101.115422

I. INTRODUCTION

In the past few decades, two-dimensional superconductivity has attracted intense research interest in understanding the nature of superconducting states and continuous phase transitions [1,2]. In recent years, a number of synthetic methods and fabrication techniques, including mechanical exfoliation, ionic-liquid gating, molecular beam epitaxy (MBE), and chemical vapor deposition (CVD), have been developed for obtaining high-quality crystalline two-dimensional (2D) superconductors [3–6]. These 2D crystalline superconductors have offered great possibilities to observe interesting quantum phenomena such as Ising paring [7], quantum Griffiths singularity [8], topological superconductivity [9,10], and anomalous metallic phase [2,4].

Depending on the growth methods and conditions, there exists a variety of morphologies in 2D materials such as domain boundaries, wrinkles, and network structures, which could significantly affect the electrical and mechanical performance of materials and devices [11–13]. In particular, there has been a considerable interest in a network of superconducting island system for studying the superconductor-to-insulator transitions [1,2]. In the early works on granular or disordered amorphous superconducting films, unusual transport properties such as reentrant behavior and negative magnetoresistance have been observed, which have been attributed to the interplay of localization and superconducting correlation [14–18]. One can describe the transition behavior in granular superconductors with the model of grains connected via Josephson-type weak links. In terms of the picture of coupled Josephson junctions, the observed resistive superconducting transition can be interpreted as a combination of Josephson and quasiparticle tunneling processes between a network of superconducting islands [19–22]. However, strong disorder is present in such superconducting systems, usually exhibiting an insulating or localization behavior at low temperatures. The effect of disorders limits the understanding on the intrinsic mechanism, and the nature of transition behavior is still a long debated topic. Recently, the rapid progress in 2D materials and nanofabrication techniques has enabled the realization of 2D artificial superconducting networks or hybrid materials, providing a novel platform to study superconducting correlations and quantum phase transitions [23–26]. Understanding the characteristic superconducting transitions in network structures may shed light on the superconductor-metal transition in 2D superconducting systems [27]. Despite these investigations, the impact of morphology on superconductivity in crystalline 2D superconductors is rarely explored. Recently, we have synthesized a series of high-quality ultrathin transition metal carbides (TMCs) crystals including Mo_2C, TaC, and WC, by means of the CVD method [6,28,29]. The 2D character of the superconductivity has been demonstrated in α-Mo_2C crystals [6]. It was found that the transport properties of these ultrathin crystals are highly reproducible and stable under ambient conditions, resulting from the covalent bonds between transition metal and carbon

*Corresponding author: wcren@imr.ac.cn
†Corresponding author: nkang@pku.edu.cn

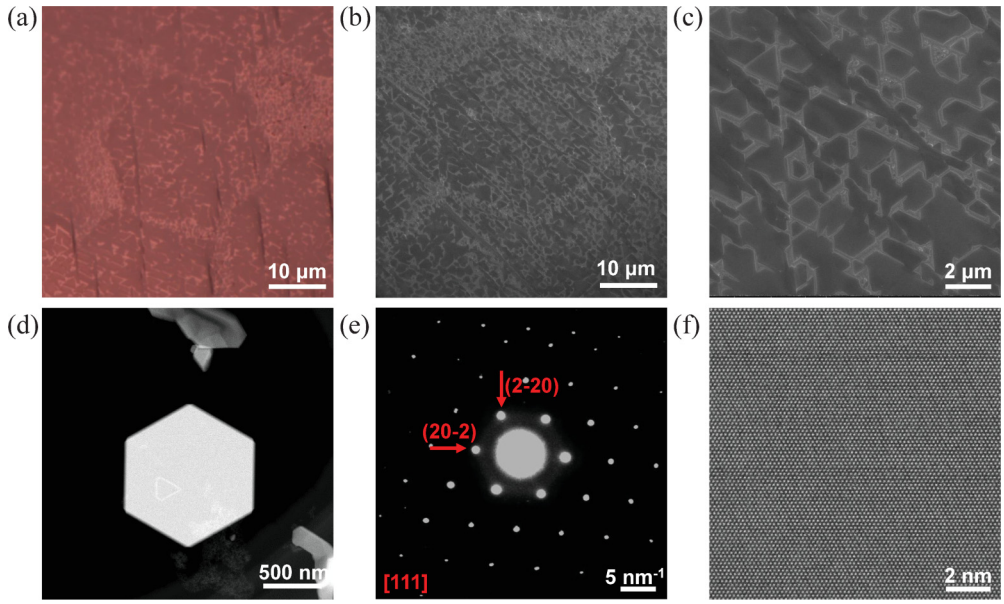

FIG. 1. (a) Optical image of reticular 2D NbC crystals on growth substrate. (b) Low magnification and (c) high magnification SEM images of the reticular NbC crystals on growth substrate. (d) Low magnification HAADF-STEM image of a hexagonal 2D NbC crystal transferred onto TEM grid. (e) Corresponding SAED pattern and (f) high-resolution HAADF-STEM image of an individual 2D NbC crystal along [111] zone axis.

atoms. Therefore, these ultrathin TMCs crystals provide an attractive material platform for exploring exotic quantum phases in a clean 2D superconducting system due to their high crystallinity combined with excellent thermal and chemical stability.

In this paper we report on the low-temperature transport measurements on the thin NbC superconducting crystal networks. Angle-dependent magnetotransport measurements demonstrate the 2D character of the superconductivity in individual NbC crystals. We observe a nonmonotonic superconducting transition as a function of temperature and magnetic field, which can be related to the characteristic morphology consisting of a network of 2D NbC islands. In terms of the picture of coupled Josephson junctions, the observed transport behavior at low temperatures can be interpreted as a combination of Josephson and quasiparticle tunneling processes. We further analyze the effect of magnetic field on the superconducting transitions, revealing the existence of quantum flux-creep regime at low temperatures and small magnetic fields.

II. METHODS

The single crystalline NbC used in this study was grown by CVD, with Cu foil put on the top of Nb foil as a growth substrate, and methane (CH_4) as a carbon source at a temperature nearby 1085 °C (the melting point of copper) for 10 min. Different from the growth of 2D ultrathin Mo_2C crystals reported previously [6], the Cu/Nb substrate should be kept at a moderate temperature to avoid the serious alloying between Cu and Nb at a high temperature. Due to the mass diffusion of Nb atoms onto the surface of Cu foil, the as-obtained NbC samples have very high nucleation density with thickness ranging from 10 to 20 nm. Figures 1(a)–1(c) show the as-grown reticular NbC crystals on Cu substrates, consisting of arrays of NbC islands. Due to the high nucleation density of NbC crystals, they connect with each other forming a network structure. The structure of the individual NbC crystals was characterized by transmission electron microscopy (TEM). A hexagongal NbC was transferred onto TEM grid, as shown in Fig. 1(d). The corresponding selected area electron diffraction (SAED) pattern shows a typical sixfold rotational symmetry, which is in accord with the characteristic of that of cubic NbC along the [111] zone axis [Fig. 1(e)]. The lattice constants derived from the SAED pattern is $a = b = c = 4.50$ Å, consistent with that of cubic NbC crystal. Moreover, high-resolution high angle annular dark field-scanning transmission electron microscopy (HR-HAADF-STEM) was used to characterize the crystalline quality, as shown in Fig. 1(f). It can be seen that there are no visible defects in such a large area, showing a highly crystalline quality for NbC crystal.

For device fabrication and transport measurements, the NbC crystals were transferred onto SiO_2/Si substrates by means of the poly(methyl methacrylate)-mediated method [6]. After the transfer process, the NbC crystals were identified and located by optical microscopy. Titanium/gold (5/90 nm) electrodes were patterned on NbC crystals using standard electron beam lithography followed by electron beam evaporation of the metals. The electrical transport measurements were performed in a Physical Property Measurement System (Quantum Design DynaCool) from room temperature to 1.8 K. The four-terminal resistance was measured using the standard low-frequency lock-in technique with an excitation current of 1–5 μA at a frequency of 17.77 Hz. The magnetic field up to 3 T was applied perpendicular to the sample plane, except for the angular dependent magnetotransport measurement.

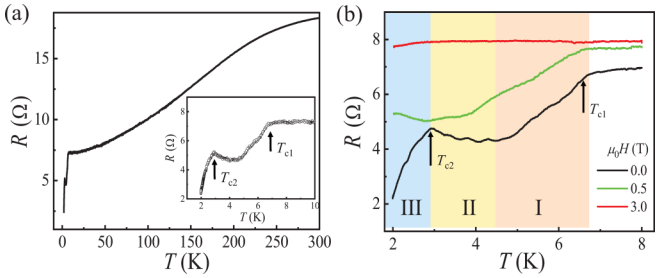

FIG. 2. (a) Temperature dependence of four-terminal resistance for a typical NbC sample with a thickness of 12 nm, measured in the temperature range of 1.8–300 K at zero magnetic field. Inset shows expanded view of $R(T)$ curve between 1.8 and 10 K, exhibiting two-step superconducting transitions. The arrows indicate two characteristic transition temperatures T_{c1} and T_{c2}, respectively. (b) Superconducting resistive transition under different applied magnetic fields of 0, 0.5, and 3.0 T, respectively. The nonmonotonic resistive transition at zero magnetic field can be divided into three temperature regions, highlighted in blue, yellow, and red backgrounds, respectively.

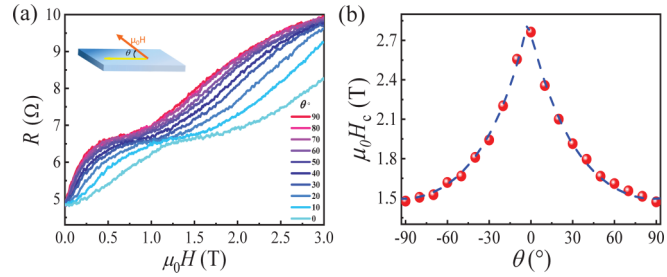

FIG. 3. (a) Magnetic field dependence of the resistance for different tilting angles θ, obtained at 1.9 K. The inset illustrates the measurement configuration. The θ is the angle between the applied field and the sample plane. As the magnetic field is titled toward the sample plane ($\theta \to 0$), the resistive transitions gradually shift to the higher magnetic fields. (b) Angle dependence of upper critical field H_c deduced from higher resistive transition region. The blue dashed line is the fitting result using the Tinkham model with Eq. (1) for 2D superconductors.

III. RESULTS AND DISCUSSION

Figure 2(a) displays the temperature-dependent four-terminal resistance $R(T)$ of a typical NbC device, measured in the temperature range of 1.8–300 K at zero magnetic field. We observe a metallic behavior upon decreasing temperature from 300 K. Reducing the temperature further, the resistance begins to drop rapidly at a critical transition temperature $T_{c1} \sim 7.0$ K, indicating the onset of superconductivity. The inset of Fig. 2(a) shows a magnified view of the resistive transition at low temperature region. A notable feature of the data is that the superconducting transition for thin NbC samples occurs via two separated stages. The resistance first drops below a normal state value at T_{c1}, and then reaches a minimum followed by an upturn below ~4.5 K, exhibiting a quasireentrant behavior ($dR/dT < 0$) [18,30,31]. As the temperature is further lowered, a second resistance drop occurs at $T_{c2} \sim 2.9$ K.

Figure 2(b) shows the resistance as a function of temperature measured under various magnetic fields $\mu_0 H$, applied perpendicular to the sample plane. The temperature evolution of the normal state resistance (above T_{c1}) remains unchanged, showing no indication of localization behavior in the normal state. A magnetic field of approximately 0.5 T completely suppresses the second resistance drop at T_{c2}, whereas the higher-temperature resistance drop at T_{c1} vanishes up to the magnetic field of ~3 T. Obviously the different response of resistance drops to the magnetic fields suggests the existence of two different transition mechanisms in the development of superconductivity in NbC networks. In contrast to the known reentrant behavior observed earlier in granular superconducting films [18,30,31] or Josephson junction arrays [32], this nonmonotonic temperature dependence of the resistive transitions can be divided by three regions, i.e., two-step drop of resistance (I, III) and resistance upturn (II), as depicted in Fig. 2(b). Similar nonmonotonic superconducting transitions as a function of temperature and magnetic field from another sample are shown in the Supplementary Material (see Fig. S1 [33]).

Before the discussion of unusual nonmonotonic superconducting transitions, we first characterize the dimensionality of the superconductivity in NbC flake by carrying out the angular dependent magnetotransport measurements. Figure 3(a) shows the magnetoresistance traces for sample 1 at various angles θ, taken at a fixed temperature of 1.9 K. The θ represents the tilt angle between the sample plane and the magnetic field direction, as illustrated in the inset of Fig. 3(a). Similar to the measured $R(T)$ curves, the magnetoresistance exhibits double-step drops as the magnetic field is decreased. As the magnetic field is titled toward the sample plane ($\theta \to 0$), both resistance drops shift to the higher magnetic fields, exhibiting a strong anisotropy of superconducting transition in NbC flakes. To characterize the higher field resistive transition originating from the thin NbC bulk crystals, we define the critical magnetic field H_c of NbC flakes as the value at which the resistance drops to 80% of the the normal state resistance. We shall discuss the resistive transition at lower magnetic fields later. Figure 3(b) presents a plot of H_c as a function of the angle θ. According to the known Tinkham model for 2D superconductors [34], the angle dependence of H_c is given by

$$\left|\frac{H_c(\theta)\sin\theta}{H_{c\perp}}\right| + \left(\frac{H_c(\theta)\cos\theta}{H_{c,\parallel}}\right)^2 = 1. \qquad (1)$$

The blue dashed line in Fig. 3(b) shows a fit to Eq. (1). It can be seen that the data can be well described by the Tinkham model, revealing the 2D character of the superconductivity in NbC flakes. Similar observations have been also reported in other 2D superconductors [6,35,36].

In order to gain an insight into the superconducting transition in the network of 2D NbC crystals, we tracked the evolution of superconducting transition under more detailed magnetic fields, as shown in Fig. 4(a). Upon increasing magnetic field, both transition temperatures (T_{c1} and T_{c2}) shift towards lower temperatures, and the quasireentrant behavior becomes smeared out gradually. It can be seen that the temperature dependence of resistive transition at lower temperatures (region III) depends strongly on the applied magnetic field below 0.5 T, in contrast to the response behavior of transition at higher temperatures (region I). The characteristic transition

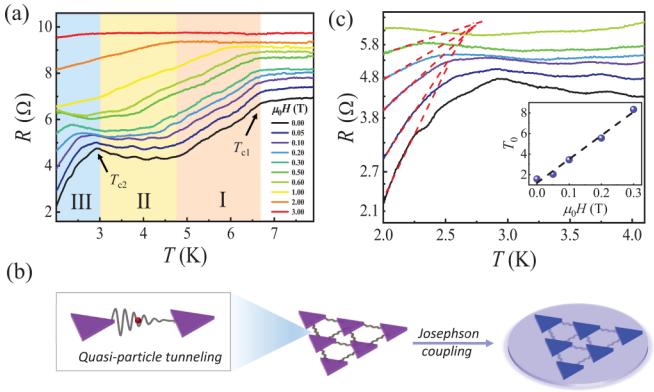

FIG. 4. (a) Resistance of two-dimensional NbC network as a function of temperature under several magnetic fields, applied perpendicular to the sample plane. (b) Schematics of the formation of Josephson junctions in the network of 2D NbC islands. The triangle shapes represent 2D superconducting NbC crystals. In an intermediate temperature regime (region II), quasiparticle tunneling between NbC islands dominates the charge transport exhibiting a quasireentrant behavior ($dR/dT < 0$). With further decreasing temperature, Josephson couplings between NbC islands become significant and global superconductivity begins to occur. (c) The semi-logarithmic plot of the resistance as as function of temperature. One can see the $R(T)$ curves at lower temperatures (region III) for various magnetic fields are in good agreement with an inverse Arrhenius relation, $R = R_0 \exp(T/T_0)$. Inset: Plot of the extracted T_0 as a function of magnetic field. The dashed line is provided as a guide for the eye, indicating a monotonically decreasing T_0 with H.

temperature ($T_{c1} \sim 7.0$ K) and corresponding critical field ($\sim$3 T) of the initial resistance drop are comparable with the reported values of large-size bulk single crystal of NbC [37,38]. Therefore, the observed resistance drop at T_{c1} (region I) can be associated with the onset of superconductivity in the individual NbC islands. To interpret the observed nonmonotonic dependence in $R(T)$, here we propose the following scenario by taking into account the 2D island morphology of our NbC samples. First, the development of local superconductivity in the individual NbC islands is accompanied by a resistance drop at T_{c1}. For our network samples, individual 2D NbC crystals are separated by grain boundaries as shown in Fig. 1, which can be modeled as superconducting weak links. With lowering temperature, the phase coherence between isolated NbC islands is strengthened due to the proximity effect. We attribute the lower transition at T_{c2} to the formation of coupled Josephson junctions between 2D NbC islands, which is expected to eventually develop global superconductivity. In the intermediate temperature regime before establishing the Josephson coupling (region II), the charge transport between islands is dominated by quasiparticle tunneling with the opening of the superconducting energy gap in NbC islands. The occurrence of quasireentrant behavior ($dR/dT < 0$) in this region can be understood due to the shrink of superconducting gap as the temperature is increased, resulting in the enhancement of the quasiparticle tunneling process. Since the Josephson coupling is more sensitive to small applied magnetic field, this scenario can explain the observation of the different response of superconducting transitions to the magnetic fields. Figure 4(b) is a schematic illustration of the transport processes in the different regimes, showing the evolution from the quasiparticle to Josephson tunneling between superconducting NbC islands as the temperature is lowered.

Having established the scenario of coupled Josephson junctions in our 2D NbC network samples, it is interesting to carry further analysis of the temperature dependence of the resistance in the Josephson coupling regime below T_{c2}. According to the thermally activated flux-creep model for 2D superconductors, the temperature-dependent resistance is expected to follow a classic Arrhenius relation. However, we found that the second drop of the resistance decreases exponentially with reducing temperature, which can best fit by $R(T) = R_0 \exp(T/T_0)$ as shown in Fig. 4(c). This unusual $R(T)$ behavior following an inverse Arrhenius law has been observed before in granular ultrathin superconducting films, and has been attributed to the model of the quantum tunneling of vortices or a percolation network of Josephson junctions [19–22]. In the inset of Fig. 4(c), we plot the extracted T_0 from the fits of $R(T)$ curves as a function of the magnetic field. It is found that T_0 exhibits a monotonic decrease with H. For our 2D superconducting crystals network, the effect of magnetic field on the resistive transition in the Josephson coupling regime is twofold. First, the magnetic field penetrates into the junction region in the form of vortices, leading to the destruction of the superconducting phase difference and Josephson coupling between NbC crystals. Second, the resistive transition below T_{c2} is associated with the development of Josephson junction between individual NbC crystals, whose coupling energy E_J is given by [39]

$$E_j = \frac{\pi h}{4e^2}\frac{\Delta}{R_N}\tanh\frac{\Delta}{2k_B T}, \tag{2}$$

where Δ is the superconducting energy gap, and R_N is the normal state resistance of junction. As the magnetic field is increased, the superconducting gap Δ is gradually suppressed, resulting in a subsequent suppression of effective Josephson coupling of the NbC network.

We next turn to the magnetoresistance measurements on the network of 2D NbC crystals. In Fig. 5(a) we present the resistance of sample 2 as a function of magnetic field at various fixed temperatures between 1.9 and 7.0 K. For clarity, the individual traces are successively shifted vertically with respect to the data at 1.9 K. It can be clearly seen that the resistance curves exhibit a nonmonotonic dependence on magnetic field at low temperatures: the resistance begins to rise and shows a peaklike feature followed by a resistance drop, and then increases at higher fields to the normal state value. Upon increasing temperature, the magnetoresistance peak, denoted by H^*, gradually moves to lower fields and eventually disappears above 4 K. It can be seen that the magnetic field-driven transition bears a strong resemblance to the temperature-dependent resistive transition in Fig. 2. It should be noted that the magnetoresistance peaks appear in the temperature range below $\sim$4 K, in which the Josephson couplings between superconducting NbC islands begin to develop as discussed above. Therefore, the observed nonmonotonic magnetoresistance behavior at low temperatures can be also interpreted qualitatively as a combination of Josephson and

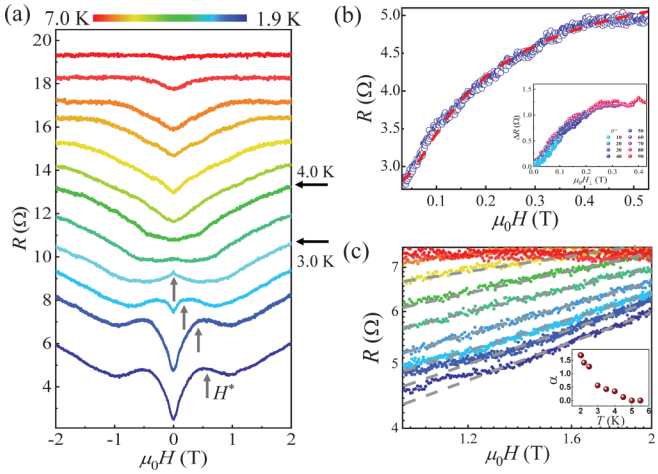

FIG. 5. (a) Magnetoresistance curves of two-dimensional NbC network at various temperatures from 1.9 to 7.0 K. The curves are successively shifted vertically for clarity. The arrows indicate the appearance of the resistance peak below 3 K, exhibiting a nonmonotonic dependence on magnetic field. With increasing temperature, the resistance peak is shifted towards zero magnetic field. (b) Low-field magnetoresistance at 1.9 K. The red solid line is a fit to the data using the quantum flux-creep model according to Eq. (3). Inset: Low-field resistance as a function of perpendicular component of magnetic field at various tilting angles θ for sample 1. (c) High magnetic field portion of the measured $R(H)$ curves from 1 to 2 T at various temperatures, plotted on a log-log scale. The dashed lines are guides to the eye, indicating a power-law dependence H^{α}. Inset: The obtained power-law exponent α as a function of temperature.

quasiparticle tunneling processes. For $H < H^*$, an increase of the resistance arises from the suppression of the Josephson couplings between the superconducting NbC islands. As H is further increased, the Josephson couplings are destroyed and Cooper pairs are localized inside the individual NbC islands. In the intermediate magnetic field region, quasiparticle tunneling through a series of islands dominates the charge transport. The drop of resistance can be attributed to a magnetic field-induced reduction of the superconducting gap, which leads to a suppression of density of states and enhances the tunneling process. A similar two-step superconducting transitions feature and scenario were also previously reported in granular disordered superconductors [14–16,40]. However, in the previous study, the granularity and the effect of disorder play important roles in the transport properties of superconductors. The normal state resistance in those disordered superconducting systems is always found to exhibit an increase with decreasing temperature [14–16,40], which is different from our observations in uniform and ultrathin NbC crystals.

Finally, we perform a quantitative analysis of the magnetic field dependence of the resistance data. As we discussed above, the transport through these 2D NbC networks at low temperatures and magnetic fields is governed by the Josephson coupling between individual crystals. When applying a magnetic field, vortices are introduced within the junction regions resulting in the destruction of Josephson coupling. It has been theoretically established that the magnetoresistance of an inhomogeneous network of superconducting islands can be expressed as [41]

$$R_{\rm sheet} \sim \frac{\hbar}{4e^2}\frac{\kappa}{1-\kappa}, \quad \kappa \sim \exp\left\{C\frac{\hbar}{e^2}\frac{1}{R_{\rm N}}\left(\frac{H-H_{c2}}{H}\right)\right\}, \quad (3)$$

where R_N is the normal state resistance and C is a dimensionless constant. Figure 5(b) show the measured $R(H)$ at 1.9 K and the best fit to Eq. (3), in good agreement with the quantum flux-creep model [41]. The magnetoresistance data and corresponding fits for temperatures 2.0, 2.2, and 2.5 K are shown in the Supplementary Material (see Fig. S2 [33]). Similar experimental results were also recently reported in other two-dimensional superconducting systems [3,4]. Additionally, the above scenario is also further examined by the measurements of the angle dependence of the magnetoresistance. Since the planar Josephson junctions are formed between 2D NbC crystals, the Josephson coupling is expected to be sensitive only to the perpendicular component of the applied field penetrating into the junction area. In the inset of Fig. 5(b), after subtracting the $\theta = 0$ trace, we plot the measured resistance at 1.9 K as a function of the perpendicular component of the magnetic field $H_{\perp} = H\sin\theta$ for the corresponding tilt angles. We found that all the magnetoresistance traces in the low-field region can be collapsed onto a single curve, consistent with the picture of Josephson-coupled 2D NbC islands at low fields.

For transitions at higher magnetic fields ($H > 1$ T), we plot the resistance as a function of magnetic field on a double logarithmic scale in Fig. 5(c). One can see that each curve shows approximate power-law behavior $R \sim H^{\alpha}$, as indicated by the dashed lines. In the framework of collective flux-creep transport model [42,43], resistive dissipation under magnetic fields arises from thermally assisted hopping of the vortices over the pinning energy. In 2D superconductors, the vortex-pinning energy barrier is expected to follow a logarithmic dependence on the magnetic field, leading to a power-law variation of the resistance with the magnetic field. Similar power-law behavior of magnetoresistance had been reported in superconducting films [44–47] and high-T_c superconductors [48–50]. The inset of Fig. 5(c) shows the temperature dependence of the exponent α, obtained from the fits of $R(H)$ curves. We found that $\alpha(T)$ exhibits a monotonic decrease with increasing T, consistent with the collective flux-creep model [42,43,46]. It should be noted that a type of power-law $R \sim H^{\alpha}$ behavior was also observed recently in other crystalline 2D superconductors [4,51], where it was attributed to the emergence of a Bose-metal phase. The connection of this exotic metallic phase to our present results in 2D NbC crystals requires further investigation.

IV. CONCLUSION

In conclusion, we have presented results on studies of electron transport through a network of thin NbC superconducting crystals. The 2D nature of the superconductivity in individual NbC crystals is evidenced by the angle-dependent magnetotransport measurements. The superconducting transitions for thin NbC samples were found to occur

via two separated stages, exhibiting a different response to the magnetic fields. We demonstrated that the observation of nonmonotonic superconducting transitions can be understood in terms of the gradual transition from the onset of local superconductivity in individual crystals to coupled Josephson junctions built between 2D NbC islands as the temperature is decreased. Moreover, further analysis of the magnetotransport data reveals an existence of quantum flux-creep regime at low temperatures and small magnetic fields in such thin NbC superconducting crystals. Our results indicate that the morphology has significant influence on the transport properties of 2D superconducting crystals, enriching the understanding of the superconducting transitions and vortex states in superconducting islanded system.

ACKNOWLEDGMENTS

We thank J. J. Zhao, J. W. Fan, and X. S. Wu for experimental support. This work was supported by the National Natural Science Foundation of China (Grants No. 11774005, No. 11974026, No. 51521091, and No. 51802314), the National Key Research and Development Program of China (Grants No. 2016YFA0300601 and No. 2017YFA0303304), and the Strategic Priority Research Program of Chinese Academy of Sciences (Grant No. XDB30000000). Dr. C. Xu acknowledge the support of the Youth Innovation Promotion Association of Chinese Academy of Sciences (Grant No. 2018223).

M.H. and C.X. contributed equally to this work.

[1] A. M. Goldman, Superconductor-insulator transitions of quench-condensed films, Low Temp. Phys. **36**, 884 (2010).

[2] A. Kapitulnik, S. A. Kivelson, and B. Spivak, Colloquium: Anomalous metals: Failed superconductors, Rev. Mod. Phys. **91**, 011002 (2019).

[3] Y. Saito, Y. Kasahara, J. Ye, Y. Iwasa, and T. Nojima, Metallic ground state in an ion-gated two-dimensional superconductor, Science **350**, 409 (2015).

[4] A. W. Tsen, B. Hunt, Y. D. Kim, Z. J. Yuan, S. Jia, R. J. Cava, J. Hone, P. Kim, C. R. Dean, and A. N. Pasupathy, Nature of the quantum metal in a two-dimensional crystalline superconductor, Nat. Phys. **12**, 208 (2016).

[5] Y. Saito, T. Nojima, and Y. Iwasa, Highly crystalline 2D superconductors, Nat. Rev. Mater. **2**, 16094 (2016).

[6] C. Xu, L. B. Wang, Z. B. Liu, L. Chen, J. K. Guo, N. Kang, X. L. Ma, H. M. Cheng, and W. C. Ren, Large-area high-quality 2D ultrathin Mo_2C superconducting crystals, Nat. Mater. **14**, 1135 (2015).

[7] X. Xi, Z. Wang, W. Zhao, J.-H. Park, K. T. Law, H. Berger, L. Forró, J. Shan, and K. F. Mak, Ising pairing in superconducting $NbSe_2$ atomic layers, Nat. Phys. **12**, 139 (2016).

[8] Y. Xing, H.-M. Zhang, H.-L. Fu, H. Liu, Y. Sun, J.-P. Peng, F. Wang, X. Lin, X.-C. Ma, Q.-K. Xue, J. Wang, and X. C. Xie, Quantum Griffiths singularity of superconductor-metal transition in Ga thin films, Science **350**, 542 (2015).

[9] H.-H. Sun, K.-W. Zhang, L.-H. Hu, C. Li, G.-Y. Wang, H.-Y. Ma, Z.-A Xu, C.-L. Gao, D.-D. Guan, Y.-Y. Li, C.-H. Liu, D. Qian, Y. Zhou, L. Fu, S.-C. Li, F.-C. Zhang, and J.-F. Jia, Majorana Zero Mode Detected with Spin Selective Andreev Reflection in the Vortex of a Topological Superconductor, Phys. Rev. Lett. **116**, 257003 (2016).

[10] M. Liao, Y. Zang, Z. Guan, H. Li, Y. Gong, K. Zhu, X.-P. Hu, D. Zhang, Y. Xu, Y.-Y. Wang, K. He, X.-C. Ma, S.-C. Zhang, and Q.-K. Xue, Superconductivity in few-layer stanene, Nat. Phys. **14**, 344 (2018).

[11] P. Y. Huang, C. S. Ruiz-Vargas, A. M. van der Zande, W. S. Whitney, M. P. Levendorf, J. W. Kevek, S. Garg, J. S. Alden, C. J. Hustedt, Y. Zhu, J. Park, P. L. McEuen, and D. A. Muller, Grains and grain boundaries in single-layer graphene atomic patchwork quilts, Nature (London) **469**, 389 (2011).

[12] G. H. Lee, R. C. Cooper, S. J. An, S. Lee, A. van der Zande, N. Petrone, A. G. Hammerherg, C. Lee, B. Crawford, W. Oliver, J. W. Kysar, and J. Hone, High-strength chemical-vapor deposited graphene and grain boundaries, Science **340**, 1073 (2013).

[13] W. J. Zhu, T. Low, V. Perebeinos, A. A. Bol, Y. Zhu, H. G. Yan, J. Tersoff, and P. Avouris, Structure and electronic transport in graphene wrinkles, Nano Lett. **12**, 3431 (2012).

[14] A. Gerber, T. Grenet, M. Cyrot, and J. Beille, Double-Peak Superconducting Transition in Granular L-M-Cu-O (L=Pr,Nd,Sm,Eu,D; M=Ce,Th) Superconductors, Phys. Rev. Lett. **65**, 3201 (1990).

[15] A. Gerber, T. Grenet, M. Cyrot, and J. Beille, Nonmonotonic resistivity transitions in granular superconducting ceramics, Phys. Rev. B **43**, 12935 (1991).

[16] I. S. Beloborodov, A. V. Lopatin, V. M. Vinokur, and K. B. Efetov, Granular electronic systems, Rev. Mod. Phys. **79**, 469 (2007).

[17] E. Zaken and R. Rosenbaum, Superconducting fluctuation conductivity in granular Al-Ge films above the metal-insulator transition, J. Phys.: Condens. Matter **6**, 9981 (1994).

[18] N. Hadacek, M. Sanquer, and J. C. Villégier, Double reentrant superconductor-insulator transition in thin TiN films, Phys. Rev. B **69**, 024505 (2004).

[19] Y. Liu, D. B. Haviland, L. I. Glazman, and A. M. Goldman, Resistive Transitions in Ultrathin Superconducting Films: Possible Evidence for Quantum Tunneling of Vortices, Phys. Rev. Lett. **68**, 2224 (1992).

[20] L. I. Glazman and N. Y. Fogel', Possibility of quantum tunneling of vortices in thin superconducting films, Sov. J. Low Temp. Phys. **10**, 51 (1984).

[21] Y. M. Strelniker, A. Frydman, and S. Havlin, Percolation model for the superconductor-insulator transition in granular films, Phys. Rev. B **76**, 224528 (2007).

[22] A. Frydman, O. Naaman, and R. C. Dynes, Universal transport in two-dimensional granular superconductors, Phys. Rev. B **66**, 052509 (2002).

[23] H. Q. Nguyen, S. M. Hollen, M. D. Stewart, J. Shainline, A. Yin, J. M. Xu, and J. M. Valles, Observation of Giant Positive Magnetoresistance in a Cooper Pair Insulator, Phys. Rev. Lett. **103**, 157001 (2009).

[24] S. Eley, S. Gopalakrishnan, P. M. Goldbart, and N. Mason, Approaching zero-temperature metallic states in mesoscopic

superconductor-normal-superconductor arrays, Nat. Phys. **8**, 59 (2012).

[25] H. Zheng, A. Allain, H. Arjmandi-Tash, K. Tikhonov, M. Feigel'Man, B. Sacépé, and V. Bouchiat, Collapse of superconductivity in a hybrid tin-graphene Josephson junction array, Nat. Phys. **10**, 380 (2014).

[26] C. Bøttcher, F. Nichele, M. Kjaergaard, H. Suominen, J. Shabani, C. Palmstrø, and C. Marcus, Superconducting, insulating and anomalous metallic regimes in a gated two-dimensional semiconductor-superconductor array, Nat. Phys. **14**, 1138 (2018).

[27] M. V. Feigel'man, A. I. Larkin, and M. A. Skvortsov, Quantum Superconductor-Metal Transition in a Proximity Array, Phys. Rev. Lett. **86**, 1869 (2001).

[28] C. Wang, L. Chen, Z. Liu, Z.-B. Liu, X.-L. Ma, C. Xu, H.-M. Cheng, W.-C. Ren, and N. Kang, Transport properties of topological semimetal tungsten carbide in the 2D Limit, Adv. Electron. Mater. **5**, 1800839 (2019).

[29] Z.-B. Liu, C. Xu, N. Kang, L.-B. Wang, Y.-X. Jiang, J. Du, Y. Liu, X.-L. Ma, H.-M. Cheng, and W.-C. Ren, Unique domain structure of two-dimensional α-Mo_2C superconducting crystals, Nano Lett. **16**, 4243 (2016).

[30] B. G. Orr, H. M. Jaeger, and A. M. Goldman, Local superconductivity in ultrathin Sn films, Phys. Rev. B **32**, 7586 (1985).

[31] H. M. Jaeger, D. B. Haviland, A. M. Goldman, and B. G. Orr, Threshold for superconductivity in ultrathin amorphous gallium films, Phys. Rev. B **34**, 4920 (1986).

[32] H. S. J. van der Zant, W. J. Elion, L. J. Geerligs, and J. E. Mooij, Quantum phase transitions in two dimensions: Experiments in Josephson-junction arrays, Phys. Rev. B **54**, 10081 (1996).

[33] See Supplemental Material at http://link.aps.org/supplemental/10.1103/PhysRevB.101.115422 for additional transport data from another NbC device, as well as more magnetoresistance data and corresponding fits, which include Ref. [41].

[34] M. Tinkham, in *Introduction to Superconductivity*, 2nd ed. (McGrawHill, New York, 1996), Chap. 4.

[35] Y. Kozuka, M. Kim, C. Bell, B. G. Kim, Y. Hikita, and H. Y. Hwang, Two-dimensional normal-state quantum oscillations in a superconducting heterostructure, Nature (London) **462**, 487 (2009).

[36] N. Reyren, S. Gariglio, A. D. Caviglia, D. Jaccard, T. Schneider, and J. M. Triscone, Anisotropy of the superconducting transport properties of the $LaAlO_3/SrTiO_3$ interface, Appl. Phys. Lett. **94**, 112506 (2009).

[37] B. T. Matthias and J. K. Hulm, A search for new superconducting compounds, Phys. Rev. **87**, 799 (1952).

[38] R. H Willens, E. Buehler, and B. T. Matthias, Superconductivity of transition-metal carbides, Phys. Rev. **159**, 327 (1967).

[39] K. K. Likharev, Superconducting weak links, Rev. Mod. Phys. **51**, 101 (1979).

[40] E. A. Early, C. C. Almasan, R. F. Jardim, and M. B. Maple, Double resistive superconducting transition in $Sm_{2-x}Ce_xCuO_{4-y}$, Phys. Rev. B **47**, 433 (1993).

[41] E. Shimshoni, A. Auerbach, and A. Kapitulnik, Transport through Quantum Melts, Phys. Rev. Lett. **80**, 3352 (1998).

[42] M. V. Feigel'man, V. B. Geshkenbein, A. I. Larkin, and V. M. Vinokur, Theory of Collective Flux Creep, Phys. Rev. Lett. **63**, 2303 (1989).

[43] W. R. White, A. Kapitulnik, and M. R. Beasley, Collective Vortex Motion in α-MoGe Superconducting Thin Films, Phys. Rev. Lett. **70**, 670 (1993).

[44] N. Mason and A. Kapitulnik, True superconductivity in a two-dimensional superconducting-insulating system, Phys. Rev. B **64**, 060504(R) (2001).

[45] I. Tamir, A. Doron, T. Levinson, F. Gorniaczyk, G. C. Tewari, and D. Shahar, Nonequilibrium restoration of duality symmetry in the vicinity of the superconductor-to-insulator transition, Phys. Rev. B **96**, 104513 (2017).

[46] J. A. Chervenak and J. M. Valles, Jr., Evidence for a quantum-vortex-liquid regime in ultrathin superconducting films, Phys. Rev. B **54**, R15649(R) (1996).

[47] D. Ephron, A. Yazdani, A. Kapitulnik, and M. R. Beasley, Observation of Quantum Dissipation in the Vortex State of a Highly Disordered Superconducting Thin Film, Phys. Rev. Lett. **76**, 1529 (1996).

[48] M. Inui, P. B. Littlewood, and S. N. Coppersmith, Pinning and Thermal Fluctuations of a Flux Line in High-Temperature Superconductors, Phys. Rev. Lett. **63**, 2421 (1989).

[49] E. Zeldov, N. M. Amer, G. Koren, A. Gupta, M. W. McElfresh, and R. J. Gambino, Flux creep characteristics in high-temperature superconductors, Appl. Phys. Lett. **56**, 680 (1990).

[50] G. Blatter, M. V. Feigel'man, V. B. Geshkenbein, A. I. Larkin, and V. M. Vinokur, Vortices in high-temperature superconductors, Rev. Mod. Phys. **66**, 1125 (1994).

[51] L.-J. Li, C. Chen, K. Watanabe, T. Taniguchi, Y. Zheng, Z. Xu, V. M. Pereira, K. P. Loh, and A. H. C. Neto, Anomalous quantum metal in a 2D crystalline superconductor with electronic phase nonuniformity, Nano Lett. **19**, 4126 (2019).